Dimer-Mediated Cation Diffusion in the Stoichiometric Ionic Conductor Li_3N

Alex D. Mulliner[1], Peter D. Battle[1,*], William I. F. David[1,2,*] and Keith Refson[2,3]

1. Inorganic Chemistry Laboratory, Oxford University, South Parks Road, Oxford, OX1 3QR, U. K.

2. ISIS Facility, Rutherford Appleton Laboratory, Chilton, Oxfordshire, OX11 0QX, U. K.

3. Department of Physics, Royal Holloway, University of London, Egham, TW20 0EX, U. K.

* Author to whom correspondence should be addressed:

peter.battle@chem.ox.ac.uk

bill.david@stfc.ac.uk

Abstract

Non-equilibrium molecular dynamics has been used to model cation diffusion in stoichiometric Li_3N over the temperature range $50 < T/K < 800$. The resulting diffusion coefficients are in excellent agreement with the available experimental data. We present a detailed atomistic account of the diffusion process. Contrary to the conclusions drawn from previous studies, our calculations show that it is unnecessary to invoke the presence of a small concentration of intrinsic defects in order to initiate diffusion. The structure can be considered to consist of alternating layers of composition Li_2N and Li. As the temperature increases an increasing number of cations leave the Li_2N layers and migrate either to the interlayer space or to the Li layer. Those that move into the interlayer space form Li_2 dimers with cations in the Li_2N layers and those that move into the neighboring layer form dimers with cations therein. The two types of dimer are aligned parallel and perpendicular to [001], respectively and have lifetimes of ~3 ps. The vacancies so created facilitate rapid diffusion in the Li_2N layers and the interlayer cation motion results in slower diffusion perpendicular to the layers.

Introduction

The potential of Li_3N to serve as a lithium-conducting solid electrolyte was first recognized by Boukamp and Huggins [1] in 1976 following transport measurements conducted on polycrystalline samples. Von Alpen *et al [2]* subsequently measured the conductivity of single crystals of Li_3N and observed significant, temperature-dependent anisotropy; at 300 K the conductivity parallel to the *z* axis of the hexagonal crystal structure was two orders of magnitude lower than the value of 10^{-3} Ω^{-1} cm^{-1} measured in the perpendicular plane. They also showed that the conductivity is purely ionic in nature. The crystal structure [3], see Figure 1, consists of eclipsed layers of composition Li_2N that are separated from each other

by lithium cations that lie at the mid-point of the inter-layer N – N vector. Each nitride ion is coordinated to eight lithium cations, two, labelled as Li(1), along the *z* axis and six, labelled as Li(2), in the Li_2N planes perpendicular to that axis; each of the lithium ions in the plane is coordinated to three nitride ions. It was recognized many years ago that, in the absence of structural disorder, it is difficult to explain the high ionic conductivity of this compound. Following the analysis of single-crystal X-ray diffraction data, Schulz and Schwarz [4] reported that the occupancy of the lithium site in the Li_2N layers, usually labelled Li(2), was temperature-dependent and that 1.8(4) % of these sites were vacant at 20 °C. No occupied interstitial sites were located and the compound was therefore described as lithium deficient. Schulz and Thiemann [5] subsequently proposed that the apparent charge imbalance was compensated by the presence of N^{2-} ions or O^{2-} ions that were incorporated during crystal growth. Wahl [6] then measured the conductivity of several single-crystal samples and concluded, on the basis of vibrational spectroscopy data, that they were all contaminated with hydrogen. It was proposed that lithium vacancies were compensated by the formation of NH^{2-} anions and observed that the ionic conductivity increased with the level of contamination. Lapp *et al* [7] confirmed this result, also on single crystals, and described hydrogen-doped Li_3N as an enhanced intrinsic conductor. However, extrapolation of their data led them to suggest, in agreement with Bell *et al* [8], that pure Li_3N would also be a good ionic conductor. Many of the syntheses performed by Wahl and Lapp *et al* deliberately introduced hydrogen into the material. However, there is no satisfactory explanation of why it should be present in samples that were intended to be pure. Furthermore, subsequent structural studies using neutron diffraction [9, 10] failed to identify a significant concentration of vacancies on the lithium sub-lattice and no convincing evidence was found for the presence of charge-compensating O^{2-} or NH^{2-} anions in the polycrystalline samples used in these experiments. These structural studies have been complemented by increasingly sophisticated ^6Li and ^7Li

NMR studies that have elucidated the dynamics of the cation diffusion [11]. For example, Wang *et al [12]* have used polycrystalline samples to determine the activation energy for diffusion in the Li_2N layers to be 0.150 ± 0.009 eV, in reasonable agreement with the value determined, also using NMR spectroscopy, by Nishida *et al* [13], but less compatible with values determined from transport measurements [14].

The experimental studies described above have been accompanied by attempts to model the behaviour of lithium nitride. Wolf *et al* [15, 16] carried out an extensive molecular-dynamics (MD) simulation of stoichiometric Li_3N at temperatures of 300 and 400 K. They were able to reproduce the temperature dependence of the anisotropy in the cation motion, but the calculated transport coefficients were significantly higher than the measured values. Their simulations showed low levels of Frenkel disorder in the Li_2N layers and the presence of interstitial cations in the interplanar region at the higher temperature; the latter appeared to play a dominant role in the conductivity both parallel and perpendicular to the *z* axis. The highly-correlated cation migration mechanisms proposed by Wolf *et al* were consistent with the MD study by Ihara and Suzuki [17] and with contemporary NMR studies [18, 19]. However, later *ab initio* MD calculations by Sarnthein *et al* [20] suggested that isolated jumps dominate the cation diffusion process. Unfortunately, their calculations underestimated the diffusion coefficients measured at 800 K by an order of magnitude. Unlike Wolf *et al*, these authors introduced cation vacancies into the Li_2N layers in order to initiate diffusion. Kishida *et al* [21] used Density Functional Theory to study the defect chemistry and conductivity of Li_3N in the temperature range $300 < T/K < 800$. They found that at 300 K the dominant defects are vacancies on the Li(2) sites and interstitial cations in the inter-layer region. The latter form dumbbell-like Li_2 dimers with the cations, Li(1), occupying the inter-layer sites, a conclusion that is consistent with the model proposed by Sarnthein *et al*. At higher temperatures Kishida *et al* found evidence for the formation of additional dimers

around the ideal cation sites in the Li_2N layers. They concluded that the ionic conductivity would be essentially isotropic in stoichiometric Li_3N, but that the introduction of hydrogen introduces anisotropy. In a combined computational and experimental study Li *et al* [22] measured an activation energy of 0.427 eV and calculated, using the NEB method, an in-plane migration energy of 0.007 eV. The latter is in reasonable agreement with the work of Sarnthein *et al* [20] whereas the former differs significantly from the values measured by Wang and Nishida. The difference between the activation energy and the migration energy was taken to be the energy needed to form the defects which are necessary if conduction is to proceed.

The historical account presented above demonstrates that there are discrepancies between different sets of experimental data collected on lithium nitride, and that the composition of the material and the detailed mechanism behind the ionic conductivity are still uncertain. No computational study has reproduced the measured transport coefficients to an acceptable level of accuracy. We therefore considered it timely to undertake a new study of stoichiometric lithium nitride using modern computational methods, namely non-equilibrium molecular dynamics (NEMD) [23], in an attempt to resolve some of these issues. A NEMD simulation increases the rate of hopping events observed in a predictable manner, thus diffusion coefficients under equilibrium conditions can be determined at temperatures where very few or no diffusion events would be observed in equilibrium MD simulations. We have previously summarized the principles of the method and demonstrated its value in modelling cation diffusion in Li_2O [24]. In the present study we have modelled the diffusion of Li^+ through stoichiometric Li_3N over the temperature range $50 < T/K < 800$. NEMD is the only method that can probe diffusion in solids at 50 K using contemporary computing facilities and our results therefore constitute the most complete account to date of the evolution of the cation

transport mechanism of Li_3N through the temperature range which is most relevant to possible applications.

Computational Method

For ease of computation, the hexagonal unit cell of Li_3N was transformed to an orthorhombic cell with $a = \sqrt{3}a_{hex}$, $b = b_{hex}$ and $c = c_{hex}$. These orthogonal axes are used in the Figures and Movies referred to in the following discussion. For reference purposes, [001] and [010] projections of the structure are shown in Figure 2. The supercell used for all the NEMD simulations presented was a 4x4x4 array of these orthorhombic cells containing a total of 128 formula units (512 atoms) with dimensions 25.3846 x 14.6558 x 15.5172 Å. The use of too small a cell with periodic boundary conditions would introduce errors caused by finite-size effects. The optimum size of the supercell was therefore determined by performing a series of simulations using supercells having different sizes and then calculating the diffusion coefficients. Test calculations using a 12 x 4 x 4 supercell at 400 K showed that when a 4 x 4 x 4 cell was used, the errors due to finite-size effects were not greater than 11 %.

The NEMD simulations were performed using a version of the CP2K package [25] that had been modified [26] to include the colour-diffusion algorithm of Evans *et al* [23]. Use of the colour-diffusion algorithm as implemented necessitates the use of a Gaussian isokinetic thermostat. The integration of the equations of motion was performed with a 1 fs time step in order to minimize the drift in conserved quantities. Simulations were run for 100 ps after an initial 10 ps equilibration period. The forces used in the NEMD calculations were calculated from a Buckingham potential that defines the interaction energy between atoms *i* and *j* as:

$$V_{ij}(r_{ij}) = \frac{q_i q_j}{r} + A_{ij} \exp\left|\frac{r_{ij}}{B}\right| - \frac{C_{ij}}{r^6}$$

The Coulombic term dominates the long range interactions and short range interactions are dominated by the parameterized terms; values of the latter were taken from Wolf *et al* [15].

In order to model diffusion perpendicular to and within the *ab* plane the NEMD colour field [23] was applied along the [001] and [100] directions, respectively. The lithium ions in alternating –(Li_2N – Li)– double layers were assigned colour charges of +1 and -1. NEMD simulations were performed using three different colour-field strengths at each of eleven temperatures in the range $50 < T/K < 800$. Care was taken to ensure that the response was directly proportional to the field strength, and that extrapolation to equilibrium conditions, i.e. the absence of a colour field, was therefore valid. The lithium diffusion coefficients along and perpendicular to [001] were calculated from the atomic displacements using the method described previously by Aeberhard *et al* [26].

Results

The diffusion coefficients calculated for lithium-ion transport within and perpendicular to the (001) planes of stoichiometric Li_3N are shown in Figure 3. The results of the experimental determination by Wang *et al* [12] are also shown and the agreement is excellent in the temperature window where the two data sets overlap. The values calculated using FF-NEMD extend over a wider temperature range than those derived previously by other means although below ~200 K the axial diffusion is too slow to be modelled precisely, even by FF-NEMD. Our data are consistent with previous studies in indicating that diffusion is significantly faster within the planes than along [001]. We shall discuss below the different mechanisms that are operating at the atomistic level.

In order for (001) cation diffusion to occur in stoichiometric Li_3N, a lithium site must become vacant for long enough to initiate the process. Our simulations show that vacancies are created by two distinct mechanisms. In the first, a lithium cation leaves an in-plane Li(2) site

and diffuses a relatively short distance (~ 2.1 Å) through the structure at a distance *c*/4 above the Li_2N plane until it approaches a nearest-neighbour occupied Li(2) site. The approach of the diffusing cation causes the cation on this site to move a distance of ~*c*/4 into the interlayer space on the opposite side of the Li_2N layer and the atoms move as a dimer aligned, on average, along [001] with a Li – Li distance of ~2.1 Å for a period of, typically, 2.5 ps before one of them returns to the Li(2) layer and the other concomitantly moves on in the interlayer space to repeat the sequence at successive sites before eventually returning to a vacant site within the layer, the receiving vacancy having been created as a result of a separate initiation process. Extensive diffusion of lithium cations along Li(2) – Li(2) vectors in the (001) plane occurs throughout the time that vacancies exist, that is for as long as some cations are displaced by *c*/4. This mechanism of vacancy creation is illustrated in Movie 1, which shows the migration of a lithium cation to the interlayer space, brief sojourns close to two adjacent Li(2) cations (not shown), a detailed depiction of the dimer formation and motion around the third Li(2) site that is encountered and, finally, the termination of the process when the featured cation is able to return to the Li_2N layer. The diffusion trace illustrated in Movie 1 was calculated using a simulation temperature of 100 K, thus demonstrating the ubiquity of cation diffusion in this compound. The time dependence of the Li – Li distance in the dimer at 100 K, the linearity of the dimer and the orientation of the dimer with respect to [001] are shown in Figure 4. The dimer can be considered to exist for ~2.5 ps in the middle of the time window.

The second mechanism for vacancy creation in the (001) plane involves both the Li(1) and Li(2) sites and, unlike the mechanism described above, leads to diffusion along [001] as well as in the (001) plane. The formation of a Li – Li dimer is usually involved, but in this case it is aligned perpendicular to [001]. Movie 2, produced using a simulation temperature of 200 K, shows a lithium cation leave a Li(2) site and move into the Li(1) layer where it forms a

dimer with a pre-existing cation. Diffusion in the (001) plane can then proceed and the movie shows that, in this particular case, the vacated Li(2) site is almost immediately filled by a cation migrating from a different Li(2) site in the same Li_2N layer. Meanwhile the dimer rotates around the Li(1) site for, typically, 4 ps before one of the cations migrates to an Li_2N layer. Movie 2 depicts a case in which this migration is to the original layer but migration to the other neighbouring layer is also possible. In either case the receiving site has the same *x* and *y* coordinates as the originating site, hence pure [001] diffusion can occur as part of this process. The variation of the interatomic distances before, during and after the 4 ps lifetime of the dimer is shown in Figure 5. The Li – Li distance in the Li_2 unit is ~2.1 Å, compared to a Li(1) – Li(2) distance of ~2.75 Å in the absence of the dimer; it can be seen that the nitrogen atoms above and below the dimer move closer to each other to screen the increased cation – cation repulsion. No interatomic distance becomes abnormally short during the diffusion process described above. The shape and the orientation of the dimer, again at 200 K, with respect to the Li_2N layer are shown in Figure 6; it is essentially linear and horizontal throughout its lifetime. Although 4 ps is a typical dimer lifetime, there are occasions when the dimer exists for only ~0.5 ps, as illustrated in Movie 3, which was produced using a simulation temperature of 600 K. In this case, the diffusing cation moves almost directly from one Li_2N layer to the next. Note that the movies presented in this account all illustrate behaviour that was observed over the full temperature range of the simulations.

In the mechanism described above, the initiating Li ion passes close to, but not through, the centre of a triangle formed by three Li cations in the Li(1) layer; it forms a dimer with the cation to which it comes closest. Movie 4, produced using a simulation temperature of 600 K, shows an alternative mechanism for diffusion along [001] that does not involve the formation of a dimer. In this case the initiating cation passes through the edge of the $Li(1)_3$ triangle and moves directly on to the next Li_2N layer. This mechanism involves diffusion both

perpendicular and parallel to [001]. The bond lengths at 600 K between the diffusing lithium atom and the three Li(1) atoms forming the triangle are shown in Figure 7(a). The distances represented by the red and black lines are approximately constant whereas the distance represented by the blue line shows a significant change as a result of the diffusion in the *xy* plane. Comparing Figure 7(a) to Figure 5, no temporary shortening of one of the Li - Li distances, i.e. the formation of a dimer, is seen in the former whereas it can be clearly seen in the latter. Figure 7(b) shows the bond lengths between the three Li(1) atoms forming the triangle. The values remain approximately equal and do not change significantly throughout the process, whereas in the dimer-mediated interlayer mechanism shown in Movie 2, the position of one Li(1) atom changes significantly. We emphasise that dimer-mediated diffusion is observed across the full temperature range of our simulations. Diffusion along [001] without dimer formation increases with increasing temperature but is always a minor contributor to the overall diffusion coefficient.

Having described the mechanisms that operate at an atomistic level over periods of ~5 ps, we shall now consider the diffusion that results over periods of ~100 ps. The diffusion trace of a single lithium cation moving across the (001) plane at 100 K, predominantly via a series of Li(2) – Li(2) hops, is shown in Figure 8 and Movie 5. The view presented in Figure 8(b) shows that the motion is constrained almost entirely to the plane, with the selected cation making only three short-lived, $\pm c/4$ excursions out of the plane while travelling ~33 Å parallel to [100] at 400 K during the 100 ps represented in the Figure. Figure 9 and Movie 6 show the path of another cation, originally from a Li(1) site, that diffuses a significant distance along [001] during a 100 ps time window. The complete set of pathways traced out at 200 K by the lithium cations in the supercell during a time period of 10 ps is shown in Figure 10. The [001] projection, see Figure 10(a), shows a high degree of diffusion between nearest-neighbour Li(2) sites in the Li_2N plane and the density within the hexagonal windows

represents occasions when dimers have been formed in the interlayer space. The [010] projection, see Figure 10(b), shows the exchange of cations between Li(1) and Li(2) sites, the movement of cations at a height c/4 above an Li_2N plane and the extended density in the Li(1) layers that is caused by dimers forming around Li(1) sites. Figure 10 also shows that the nitride ions remain on their crystallographic sites; there is no anion diffusion.

The trajectories of all the lithium cations over the course of a 100 ps simulation at 200 K were used to create the number-density plots shown in Figure 11 which emphasise several interesting points. Figure 11(a) shows the logarithm of the lithium number density for a thin slab normal to [001] and containing the Li(1) site at $z = c/2$. The majority of the density is located at the regular Li(1) sites but a hexagonal pattern of non-zero density can be seen around these sites. This density stems from the formation of dimers in the plane perpendicular to [001]. These Li_2 dimers tend to align along Li(1) – Li(1) vectors and consequently the resulting hexagons are offset by 30 ° from those formed by Li(2) sites in the neighbouring Li_2N layers, thus minimising cation – cation repulsions. The rotation of the dimers around the hexagons can be seen in Movie 7. Figure 11(b) shows the logarithm of the lithium number density viewed along the [100] direction with Li_2N layers at the top, bottom, and middle of the colour map; the intervening layers contain Li(1) sites. As before, the highest density is found at the regular Li(2) and Li(1) sites. The Li(1) sites are surrounded by an elliptical density distribution as a consequence of the formation of horizontal dimers. The Li(2) sites show an approximately spherical density distribution but there is significant density directly between them due to the frequent hopping between nearest-neighbour sites. The density directly above and below the Li(2) sites is due to the formation of vertical dimers and density attributable to motion between these dimer sites can be seen at a distance $c/4$ above and below the Li_2N layers.

In order to provide a quantitative description of the lithium distribution within the Li_3N structure as a function of temperature the unit cell was divided into three slabs of equal thickness perpendicular to [001]. The slabs were centred on the Li(1), Li(2) and *c*/4 layers. The former contains not only the cations on the Li(1) site but also those that are involved in the formation of horizontal dimers. The slab centred at *c*/4 contains cations involved in interlayer hopping and the formation of vertical dimers, and that centred on the Li(2) site contains the remaining cations. The results of NEMD simulations were used to assign each cation to one of the three slabs and hence the time-averaged distribution of the cations was determined as a function of temperature, see Figure 12. In the ideal structure of Li_3N the Li(1) and Li(2) sites would contain 1 and 2 cations per formula unit, respectively. Figure 12 shows that as the temperature increases the Li(2) sites are depopulated with the majority of the displaced cations moving into the *c*/4 slab and a smaller fraction going into the slab containing Li(1) and the horizontal dimers. The decrease in the population of the Li(2) site with increasing temperature is entirely consistent with the increase in diffusion observed experimentally. This site is at located at (⅓, ⅔, 0) in the hexagonal unit cell. We suggest that the displaced cations predominantly occupy interstitial sites in either vertical or horizontal dimers that are located at (⅓, ⅔, ~0.24) and (~0.29, 0, ½), respectively, together with their symmetry-related sites, see Figure 13.

Discussion

Many previous studies of Li_3N have only been able to account for the high Li^+-cation conductivity by assuming that the compound is lithium deficient and therefore has an intrinsic concentration of vacancies on the mobile sub-lattice. It has usually been assumed that the resulting charge imbalance is compensated by the presence of aliovalent anions, even when there is no experimental evidence to suggest that these are present. Schulz *et al* [4, 5] ,

for example, interpreted the results of their X-ray diffraction experiment in terms of a partially-occupied cation sub-lattice but they were unable to identify the mechanism of charge compensation from their data. They therefore suggested that some N^{2-} ions were present or that O^{2-} ions were incorporated into the structure during the synthesis of the sample. The use of FF-NEMD has allowed us to reproduce computationally the observed high-temperature diffusion coefficient and the anisotropy of the diffusion in Li_3N without invoking non-stoichiometry. The calculated diffusion coefficients show that rapid cation diffusion can occur in the plane perpendicular to [001] well below room temperature. Furthermore, we have been able to elucidate in detail the atomistic mechanism behind the macroscopic diffusion. As the thermal energy increases with increasing temperature, cations are increasingly able to leave the Li(2) sites in the Li_2N layers and form Li_2 pairs with either other Li(2) cations (vertical dimers) or with Li(1) cations (horizontal dimers). These ion pairs typically have a lifetime of ~3 - 5 ps at ~200 K and during this period rapid cation diffusion can occur in the vacancy-containing Li_2N layers. A limited amount of diffusion occurs in the direction perpendicular to the layers when the displaced cation fills a vacancy in the Li_2N layer above or below its point of origin, rather than returning to the layer from which it came.

The insight into the diffusion mechanism and the level of agreement with the experimental data achieved in the present study far exceeds that achieved in previous computational studies. For example, with the limited computational resources available to them, Wolf *et al* [15, 16] deduced the presence of vacancies in the Li_2N layers and the presence of interstitial cations in the interlayer space of stoichiometric Li_3N. However, they did not obtain a detailed model of the dimer formation or a satisfactory level of quantitative agreement between their calculated transport coefficients and those determined experimentally. Sarnthein *et al* [20] proposed the formation of horizontal dimers around the Li(1) site but their calculations assumed that the compound was non-stoichiometric in order to generate vacant lithium sites.

Kishida *et al* [21] identified the formation of both the horizontal dimers and the vertical dimers around the Li(2) sites, but concluded that the anisotropy in the ionic conductivity was attributable to the presence of hydrogen impurities. No previous computational study has predicted anisotropic diffusion in stoichiometric Li_3N and reproduced the experimentally-observed diffusion coefficient with the accuracy achieved herein. Finally, we note that Sarathein *et al* [20] suggested that the poor quantitative agreement achieved by Wolf *et al* [15, 16] might have been the result of the absence of covalency from their ionic potential model. The excellent agreement achieved, using the same potential model, in the present study shows that this model does indeed provide an accurate description of the interionic interactions in Li_3N. We speculate that the discrepancy in the diffusion coefficients calculated by Wolf *et al* is most likely to be a consequence of finite-size enhancement in their smaller simulation cell although the failure to reach equilibrium in their much shorter MD runs could also be a factor.

Conclusion

The results of the present study emphasise the value of FF-NEMD, used in conjunction with a colour field, in the study of the temperature dependence of anisotropic diffusion in simple inorganic systems. By using this approach we have been able to answer many of the long-standing, fundamental questions concerning the ionic conductivity of Li_3N. More specifically, we have identified an atomistic mechanism that facilitates high, anisotropic ionic conductivity in a stoichiometric compound, *i.e.* in the absence of intrinsic defects and we have also been able to reproduce accurately the experimentally-determined diffusion coefficient.

Acknowledgments

Computing resources were provided by the UK Car-Parrinello Consortium (EPSRC Grants EP/F036809/1 and EP/K013750/1) and the e-science facility of the Science and Technology Facilities Council (STFC). A. D. M. acknowledges the STFC for financial support.

References

1. B. A. Boukamp and R. A. Huggins, *Physics Letters* **58A**, 231 (1976)
2. U. von Alpen, A. Rabenau and G. H. Talat, *Appl. Phys. Letts.* **30**, 621 (1977)
3. A. Rabenau and H. Schulz, *J. Less-Common Metals* **50**, 155 (1976)
4. H. Schulz and K. H. Schwarz, *Acta Cryst.* **A34**, 999 (1978)
5. H. Schulz and K. H. Thiemann, *Acta Cryst.* **A35**, 309 (1979)
6. J. Wahl, *Solid State Communications* **29**, 485 (1979)
7. T. Lapp, S. Skaarup and A. Hooper, *Solid State Ionics* **11**, 97 (1983)
8. M. F. Bell, A. Breitschwerdt and U. v. Alpen, *Mater. Res. Bull.* **16**, 267 (1981)
9. A. Huq, J. W. Richardson, E. R. Maxey, D. Chandra and W.-M. Chien, *J. Alloys and Compounds* **436**, 256 (2007)
10. D. H. Gregory, P. M. O'Meara, A. G. Gordon, J. P. Hodges, S. Short and J. D. Jorgensen, *Chem. Mater.* **14**, 2063 (2002)
11. M. Wilkening and P. Heitjans, *ChemPhysChem* **13**, 53 (2012)
12. Z. Wang, M. Gobet, V. Sarou-Kanian, D. Massiot, C. Bessada and M. Deschamps, *Phys. Chem. Chem. Phys.* **14**, 13535 (2012)
13. K. Nishida, T. Asai and S. Kawai, *Solid State Communications* **48**, 701 (1983)
14. U. von Alpen, *J. Solid State Chem.* **29**, 379 (1979)
15. M. L. Wolf, J. R. Walker and C. R. A. Catlow, *J. Phys. C: Solid State Phys.* **17**, 6623 (1984)
16. M. L. Wolf and C. R. A. Catlow, *J. Phys. C: Solid State Phys.* **17**, 6635 (1984)
17. S. Ihara and K. Suzuki, *Phys. Lett. A* **110**, 265 (1985)
18. R. Messer, H. Birli and K. Differt, *J. Phys. C: Solid State Phys.* **14**, 2731 (1981)

19. D. Brinkmann, M. Mali, J. Roos, R. Messer and H. Birli, *Phys . Rev. B* **26**, 4810 (1982)

20. J. Sarnthein, K. Schwarz and P. E. Blochl, *Phys . Rev. B* **53**, 9084 (1996)

21. I. Kishida, F. Oba, Y. Koyama, A. Kuwabara and I. Tanaka, *Phys . Rev. B* **80**, 024116 (2009)

22. W. Li, G. Wu, C. M. Araujo, R. H. Scheicher, A. Blomqvist, R. Ahuja, Z. Xiong, Y. Feng and P. Chen, *Energy Environ. Sci.* **3**, 1524 (2010)

23. D. J. Evans, W. G. Hoover, B. H. Failor, B. Moran and A. J. C. Ladd, *Phys. Rev. A* **28**, 1016 (1983)

24. A. D. Mulliner, P. C. Aeberhard, P. D. Battle, W. I. F. David and K. Refson, *Phys. Chem. Chem. Phys.* **17**, 21470 (2015)

25. CP2K: released under the GPL license, freely available at http://www.cp2k.org

26. P. C. Aeberhard, S. R. Williams, D. J. Evans, K. Refson and W. I. F. David, *Phys . Rev. Lett.* **108**, 095901 (2012)

Figure Captions

Figure 1 Hexagonal unit cell of Li_3N; green (red) circles represent lithium (nitride) ions.

Figure 2 Projections along (a) [001] and (b) [010] of the Li_3N structure in an orthogonal unit cell having $a = \sqrt{3}a_{hex}$, $b = b_{hex}$ and $c = c_{hex}$. Green (red) circles represent lithium (nitrogen).

Figure 3 Temperature dependence of the diffusion coefficient of lithium in Li_3N.

Figure 4 Time dependence of the bond lengths and angles in a Li_2 dimer formed around a Li(2) site at 100 K; (a) the Li – Li distance, (b) the Li – Li(2)* – Li angle (where Li(2)* represents the ideal Li(2) site) and (c) the tilt angle, δ_v, between the Li – Li vector and [001]. The dimer can be considered to exist for $2.5 < t/\text{ps} < 5$.

Figure 5 Time dependence of the bond lengths in a Li_2 dimer formed around a Li(1) site at 200 K. A colour key is provided in the lower part of the diagram. The dimer can be considered to exist for $1.5 < t/\text{ps} < 5.5$.

Figure 6 Time dependence of bond angles in a Li_2 dimer formed around a Li(1) site at 200 K; (a) the Li – Li(1)* - Li angle (where Li(1)* represents the ideal Li(1) site) and (b) the angle, δ_h, between the Li – Li vector and the Li_2N plane. The dimer can be considered to exist for $1.5 < t/\text{ps} < 5.5$.

Figure 7 Time dependence of interatomic separations when interlayer diffusion occurs at 600 K without dimer formation: (a) the separation between the diffusing Li(2) cation and three Li(1) atoms and (b) the separations between the cations in the Li_3 triangle through which the diffusing cation passes.

Figure 8 Diffusion perpendicular to [001]: the diffusion trace of a single Li^+ cation (green) through the nitride sub-lattice (red) over a period of 100 ps at 100 K viewed along (a) [001] and (b) along [010].

Figure 9 Diffusion parallel to [001]: the diffusion trace of a single Li^+ cation (green) through the nitride sub-lattice (red) over a period of 100 ps at 400 K viewed along [010].

Figure 10 (a) [001] and (b) [010] projections of the lithium (green) and nitride (red) distribution during the course of a 10 ps NEMD simulation at 200 K.

Figure 11 Sections through the lithium density distribution at 200 K shown in Figure 10 projected (a) along [001] showing only the Li(1) sites and (b) along [100] showing both the Li(1) and Li(2) sites. Blue (red) regions represent low (high) lithium density; the scale bar is logarithmic.

Figure 12 Temperature dependence of the time-averaged lithium content of the Li(2), Li(1) and *c*/4 layers in Li_3N.

Figure 13 Hexagonal unit cell of Li_3N showing the location of interstitial sites in (a) the vertical dimer and (b) the horizontal dimer. Green (red) circles represent lithium (nitride) ions on their regular sites; blue circles represent interstitial sites.

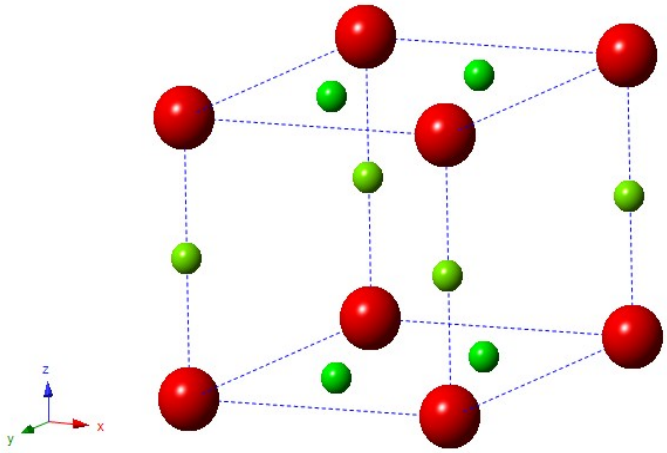

Figure 1

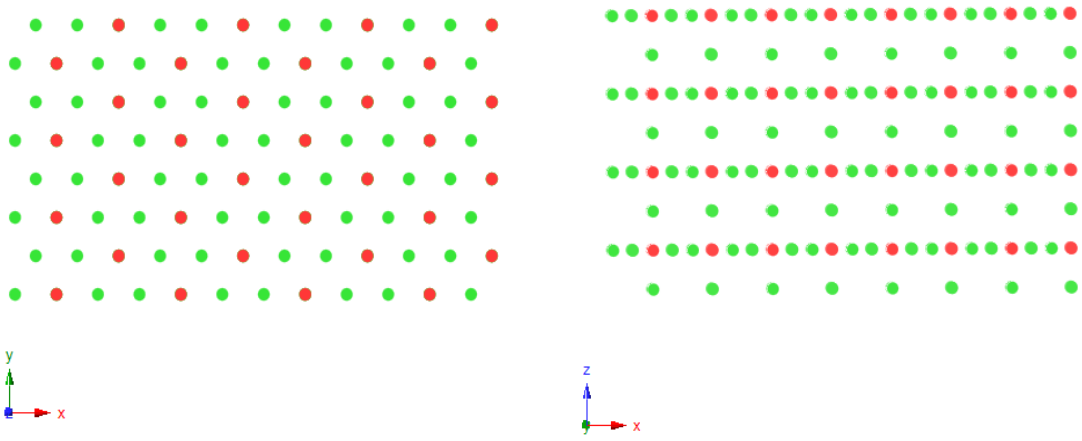

(a) (b)

Figure 2

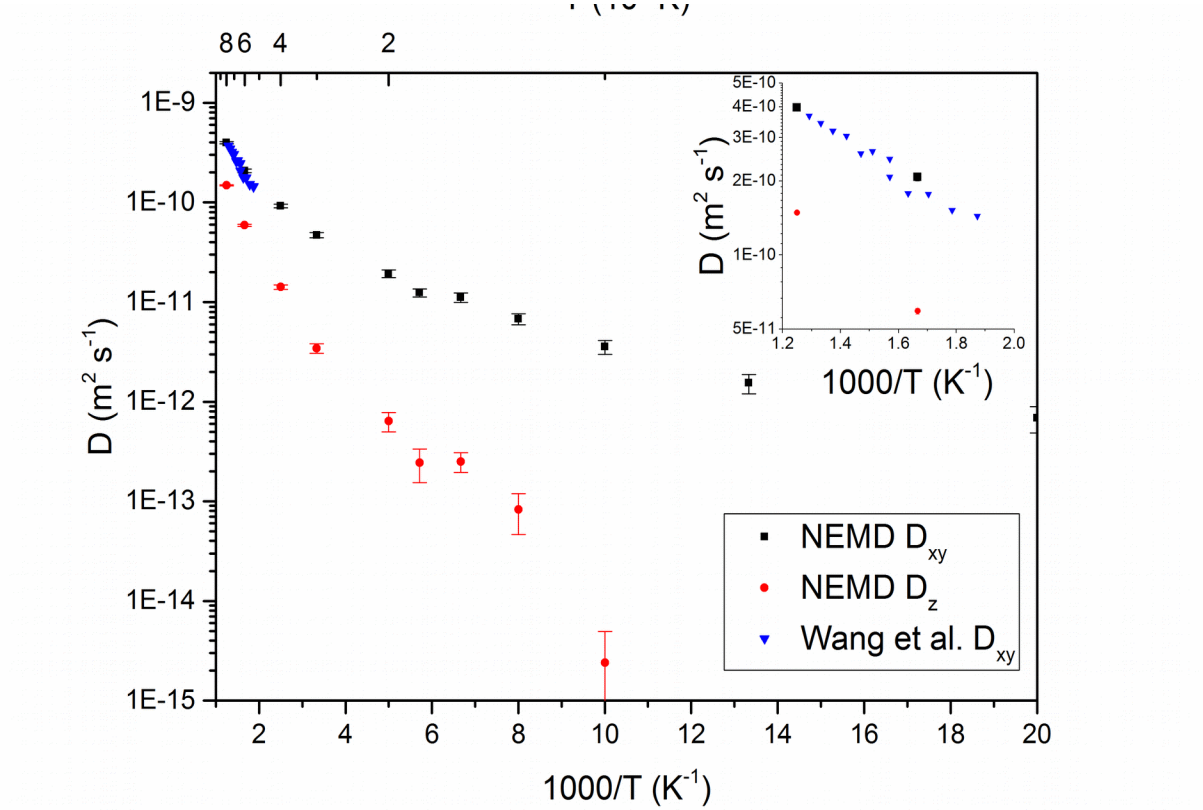
8 6 4 2
1E-9
1E-10
1E-11
1E-12
1E-13
1E-14
1E-15
D (m^2 s^{-1})
2 4 6 8 10 12 14 16 18 20
1000/T (K^{-1})
NEMD D$_{xy}$
NEMD D$_z$
Wang et al. D$_{xy}$
5E-10
4E-10
3E-10
2E-10
1E-10
5E-11
D (m^2 s^{-1})
1.2 1.4 1.6 1.8 2.0
1000/T (K^{-1})

Figure 3

(a)

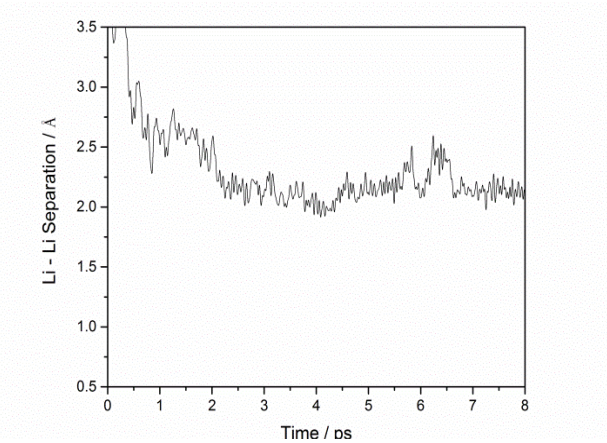
Li - Li Separation / Å
Time / ps

(b)

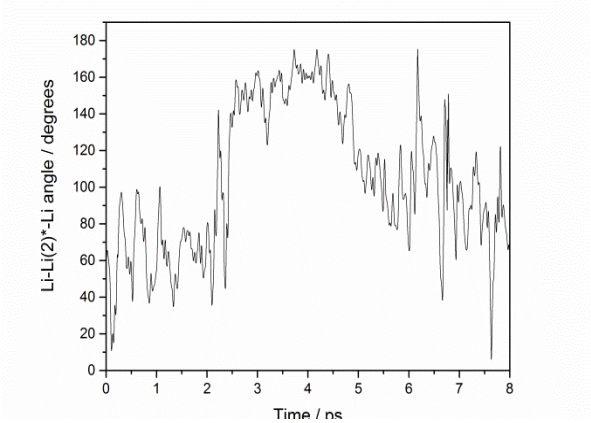
Li-Li(2)*-Li angle / degrees
Time / ps

(c)

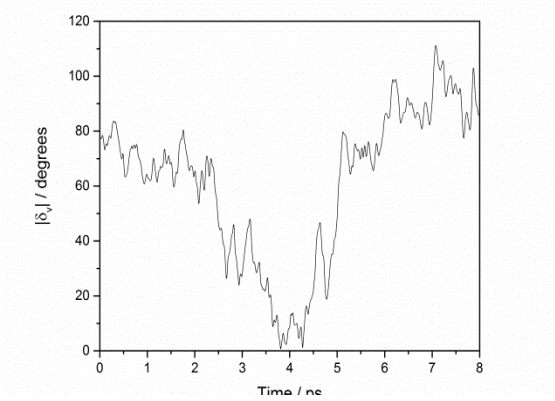
|δv| / degrees
Time / ps

Figure 4

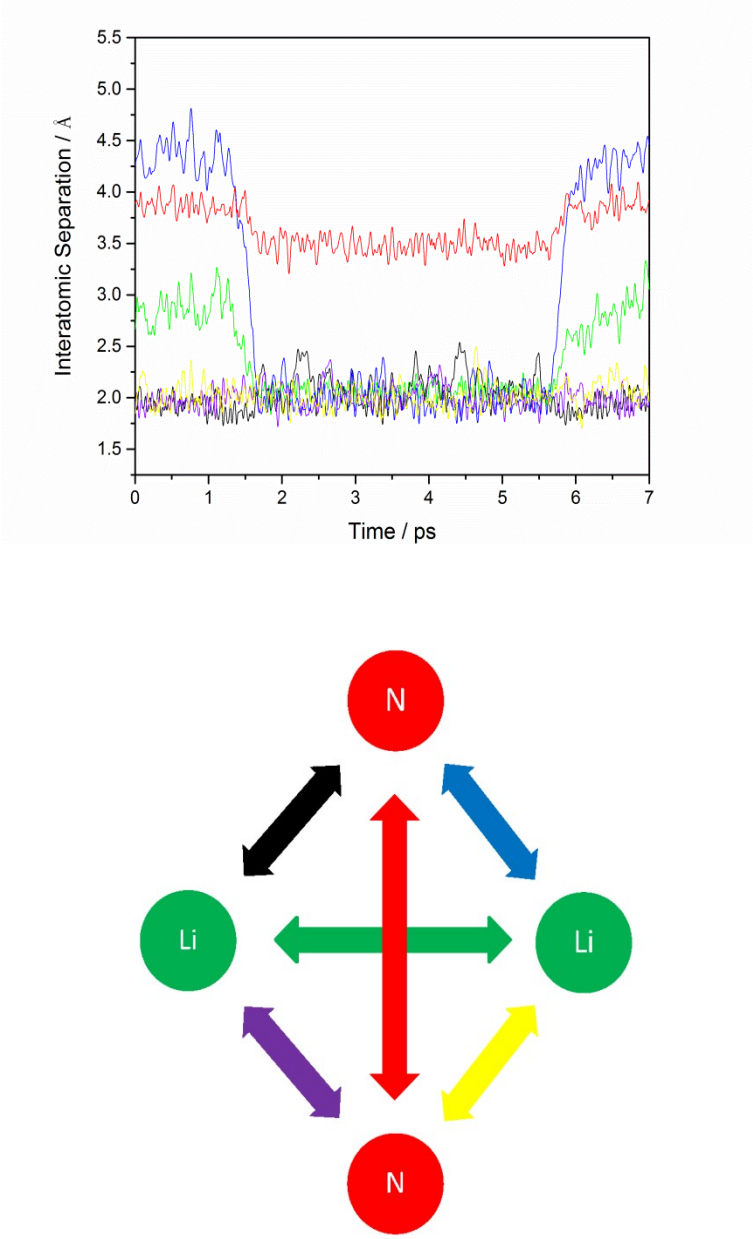
Interatomic Separation / Å
Time / ps
5.5
5.0
4.5
4.0
3.5
3.0
2.5
2.0
1.5
0
1
2
3
4
5
6
7
N
Li
Li
N

Figure 5

(a)

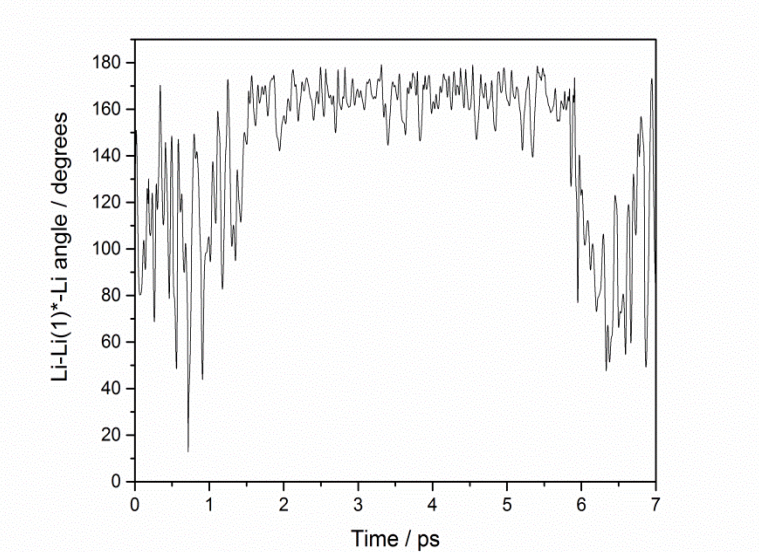
Li-Li(1)*-Li angle / degrees
Time / ps
0
20
40
60
80
100
120
140
160
180
0
1
2
3
4
5
6
7

(b)

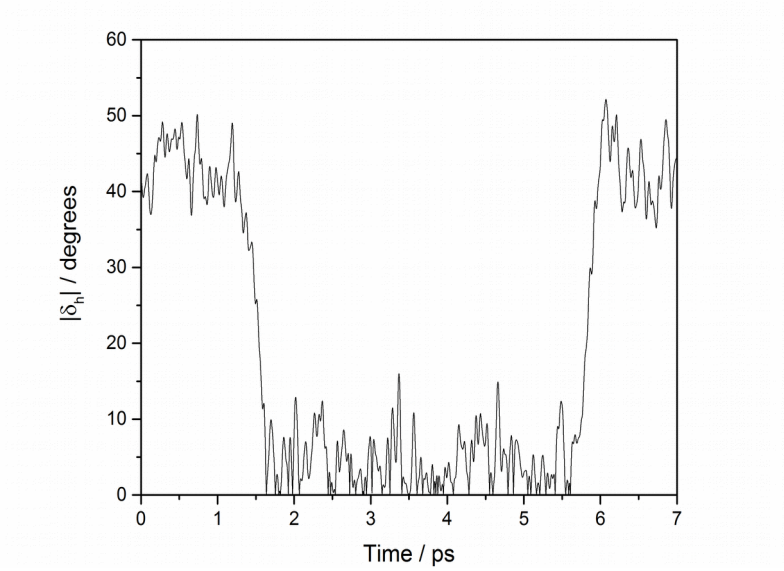
|δh| / degrees
Time / ps
0
10
20
30
40
50
60
0
1
2
3
4
5
6
7

Figure 6

(a)

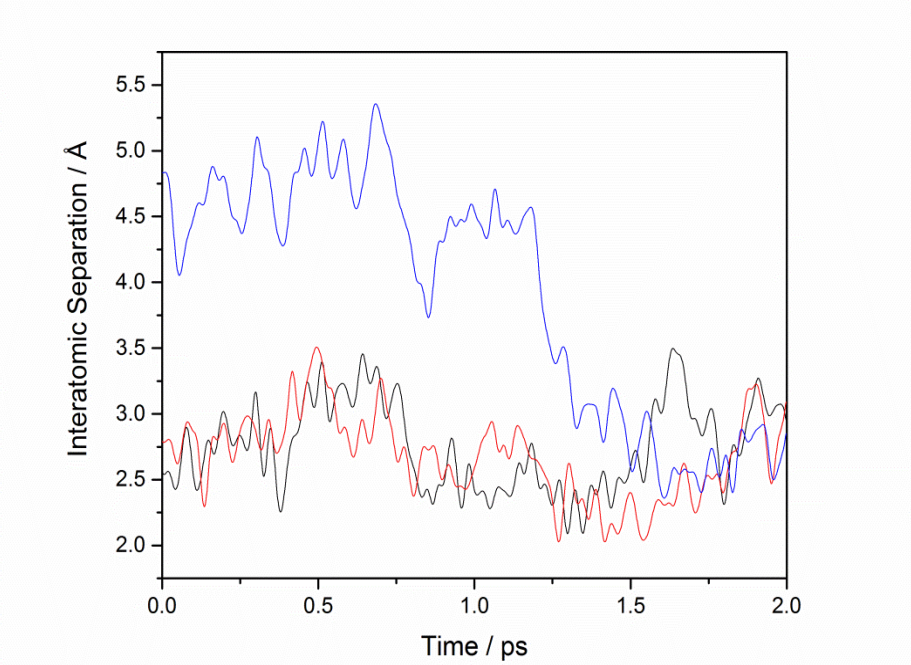
Interatomic Separation / Å
5.5
5.0
4.5
4.0
3.5
3.0
2.5
2.0
0.0
0.5
1.0
1.5
2.0
Time / ps

(b)

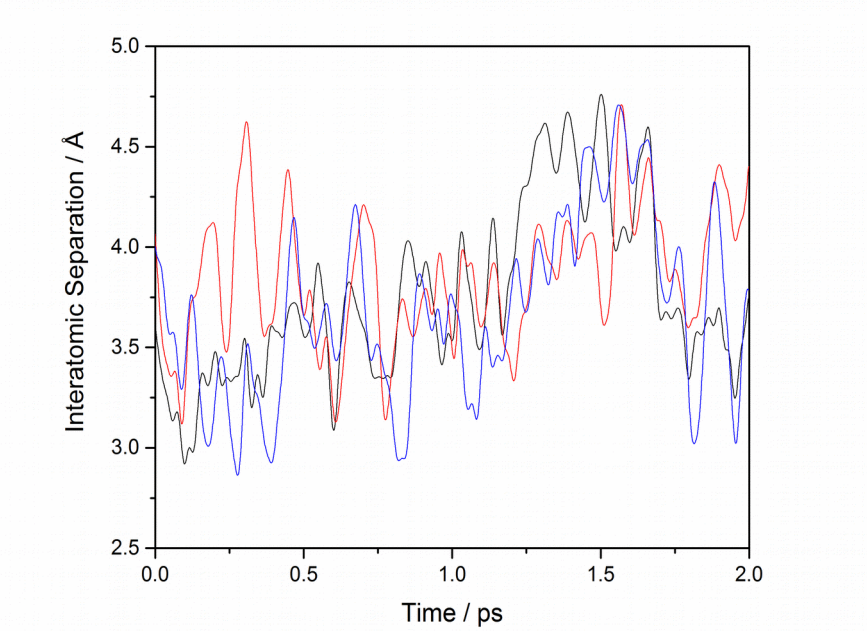
Interatomic Separation / Å
5.0
4.5
4.0
3.5
3.0
2.5
0.0
0.5
1.0
1.5
2.0
Time / ps

Figure 7

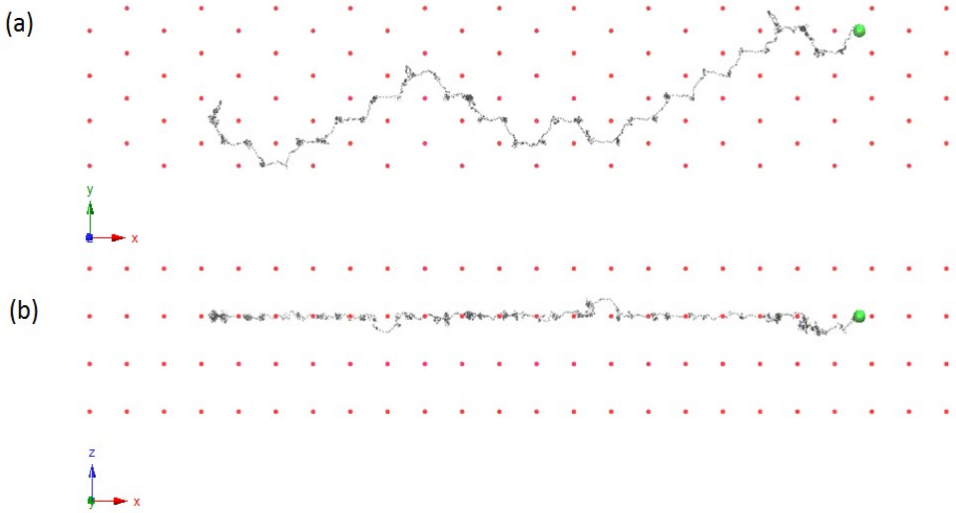

Figure 8

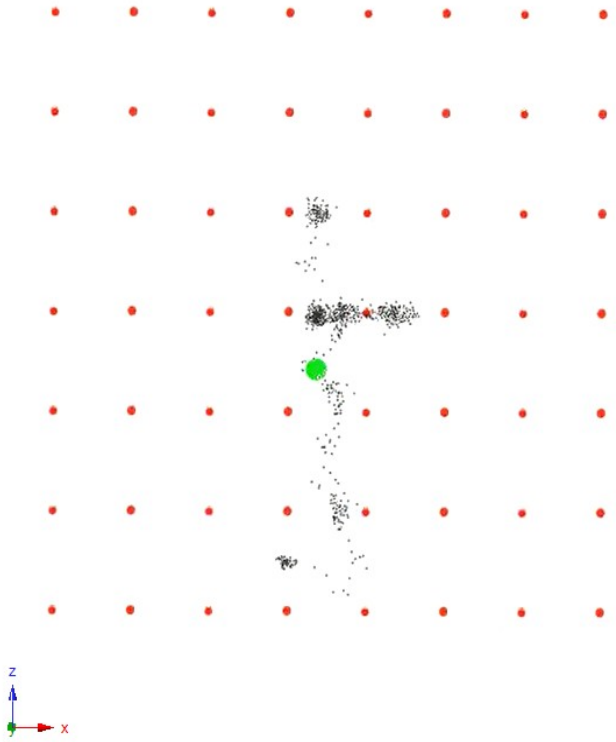

Figure 9

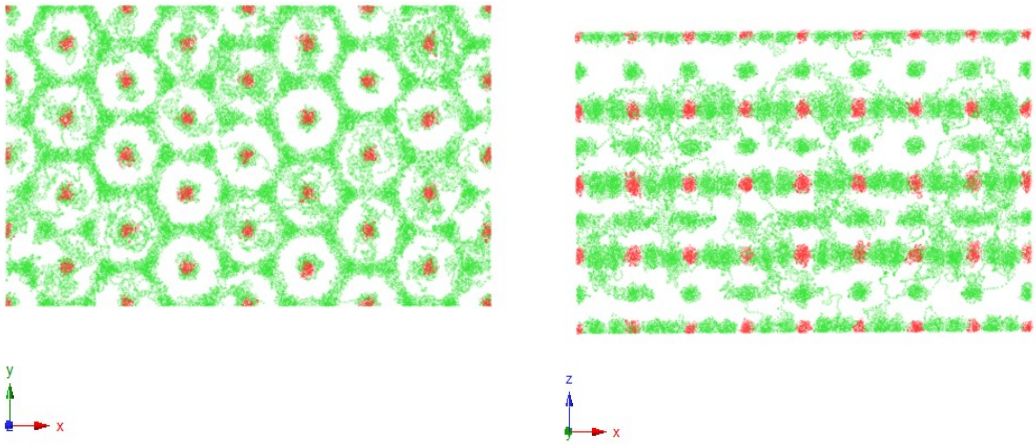

(a) (b)

Figure 10

(a)

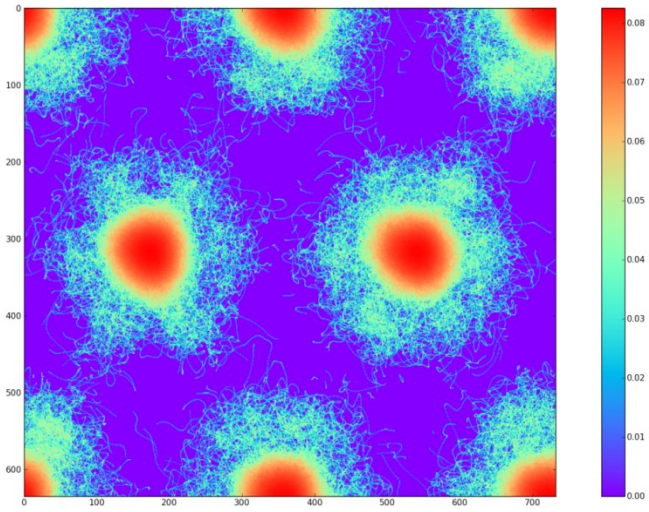
0
100
200
300
400
500
600
0
100
200
300
400
500
600
700
0.08
0.07
0.06
0.05
0.04
0.03
0.02
0.01
0.00

(b)

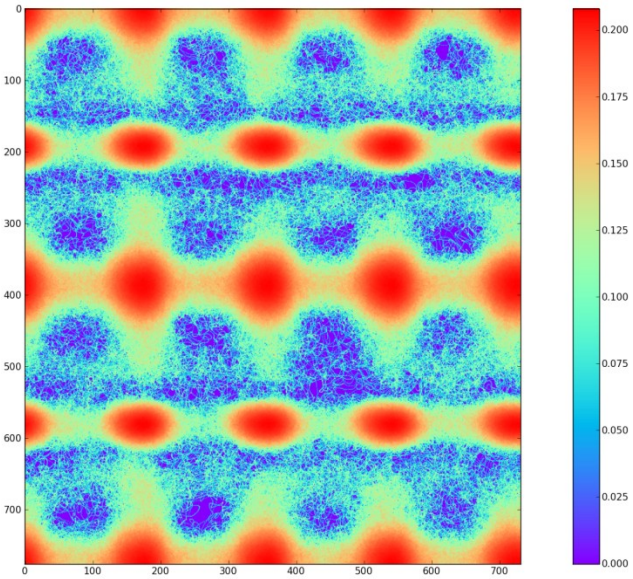
0
100
200
300
400
500
600
700
0
100
200
300
400
500
600
700
0.200
0.175
0.150
0.125
0.100
0.075
0.050
0.025
0.000

Figure 11

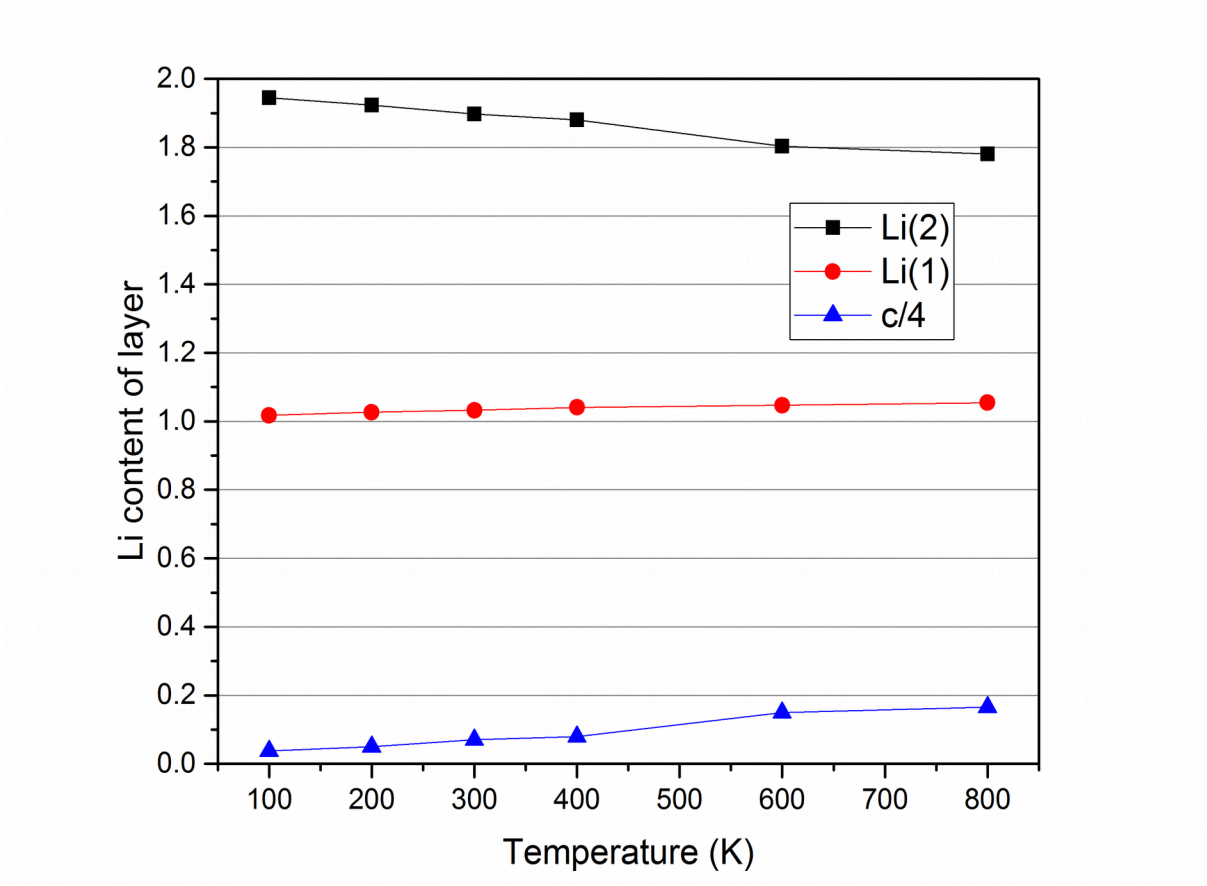
Li content of layer
Temperature (K)
Li(2)
Li(1)
c/4
2.0
1.8
1.6
1.4
1.2
1.0
0.8
0.6
0.4
0.2
0.0
100
200
300
400
500
600
700
800

Figure 12

(a)

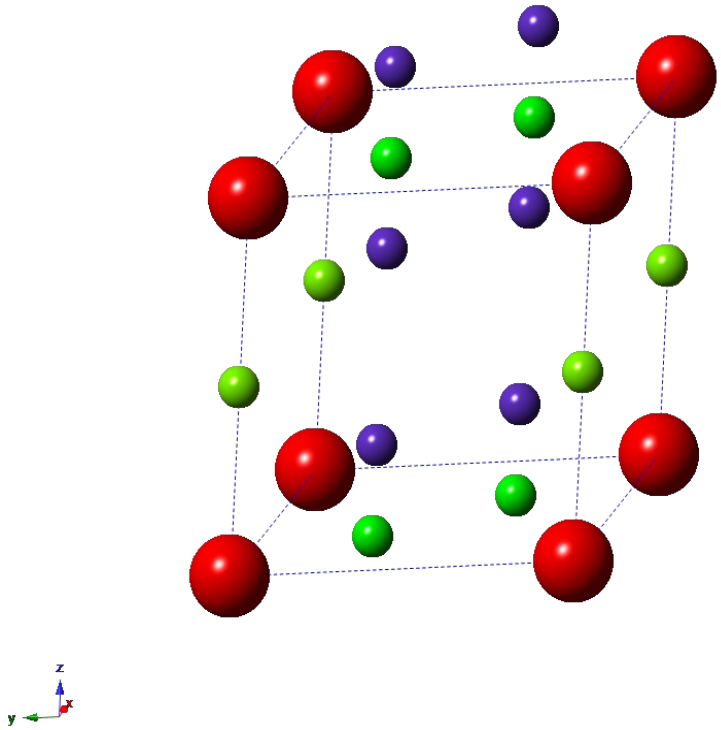

(b)

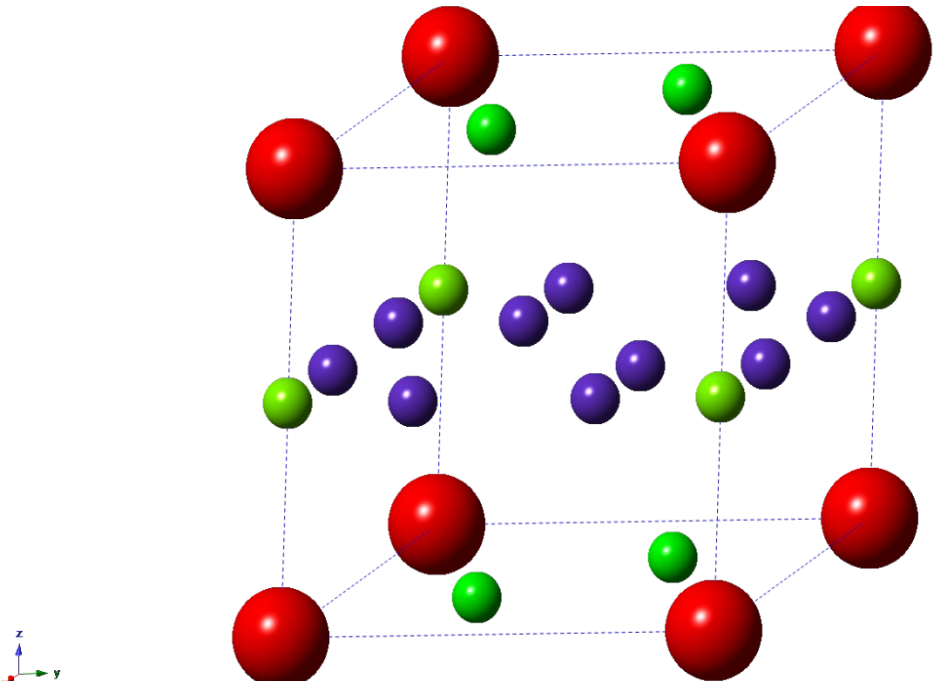

Figure 13

Movie Captions

Movie 1 [010] view showing 2.5 ps of a diffusion process at 100 K involving the formation of a vertical dimer at a Li(2) site in Li_3N. The green and blue circles represent the two Li^+ cations that form the dimer. The blue and green points are their traces with each point representing a time window of 1 fs. The red circles represent the N^{3-} anions.

Movie 2 2.7 ps of a Li^+ diffusion process at 200 K involving the formation of a horizontal dimer at a Li(1) site in Li_3N. The green and blue circles are Li^+ cations. The red circles represent the N^{3-} anions. Each point in the trace represents a time window of 1 fs.

Movie 3 2 ps of an interlayer diffusion process in Li_3N via a Li(1) site at 600 K. The red and blue circles represent N^{3-} and Li^+ ions, respectively. The green circle is the diffusing lithium atom. Each coloured point in the trace represents a 1 fs time window.

Movie 4 2.5 ps of an interlayer diffusion process in Li_3N at 600 K. The red and blue circles represent N^{3-} and Li^+ ions respectively. The green circle is the diffusing lithium atom which is seen to pass through the edge of a $Li(1)_3$ triangle. Each coloured point in the trace represents a 1 fs time window.

Movie 5 The diffusion trace of a single Li^+ cation (green) through the N^{3-} sub-lattice (red) of Li_3N over a period of 100 ps at 100 K viewed (a) along [001] and (b) along [010]. Each black point represents 100 fs of the Li^+ cation trajectory.

Movie 6 The diffusion trace of a single Li^+ cation (green) through the N^{3-} sub-lattice (red) of Li_3N over a period of 100 ps at 400 K viewed along [010]. Each black point represents 100 fs of the Li^+ cation trajectory.

Movie 7 [001] view of 2.7 ps of a Li^+ diffusion process at 200 K involving the formation of a horizontal dimer at a Li(1) site in Li_3N. The green and blue circles are Li^+ cations. The red circles represent the N^{3-} anions. Each point in the trace represents a time window of 1 fs.